Formation Sequence of Different Spinel Species in Megacrystalline Peridotites of the Udachnaya-East Kimberlite Pipe (Yakutia): Evidence for the Metasomatism of Depleted Mantle

Lyudmila Pokhilenko [ID]

V.S. Sobolev Institute of Geology and Mineralogy, Siberian Branch of Russian Academy of Science, Ak. Koptyuga 3, 630090 Novosibirsk, Russia; lu@igm.nsc.ru or blingoreluiy@yandex.ru; Tel.: +7-913-717-5391

Abstract: The large compositional variations in spinels from extremely depleted, megacrystalline harzburgite–dunites in the Udachnaya-East kimberlite pipe, Yakutia, apparently reflect multistage metasomatism. Changes in the redox regime are reflected in the compositions of different parts of mineral grains. From most reduced to most oxidized, spinel compositions divide into: (1) primary (rock-forming) Cr-spinel and spinel from the central parts of sulfide grains, (2) spinel from microcracks in olivine, (3) spinel in kelyphitic rim around garnet between garnet and olivine (Rim1 and Rim2 spinel), and (4) spinel in transformed kelyphitic rim around garnet between garnet and kimberlite (Rim3 spinel). P-T conditions for the vast majority of samples, calculated using the composition of primary Cr-spinel, fall in the diamond stability field. A change in the composition of spinels of different generations occurs along the sides of the classical triangle of spinel compositions Al–Cr–Fe^{3+}: (1) Rim2 to Rim1 spinel—Al–Cr trend, (2) primary Cr-spinel to magnetite rim in the edge—Cr–Fe^{3+} (kimberlite) trend, (3) replacing Rim1 to Rim3—Al–Fe^{3+} trend.

Keywords: spinel; megacrystalline harzburgite–dunite; kimberlite; mantle metasomatism; kelyphitic rim

1. Introduction

Spinel from different rock types has been actively studied by petrologists for many years; firstly, as a mineral, it is commonly found in different rocks and is accessible for study, and secondly, because its chemical composition can be used as a petrogenetic indicator [1–5]. However, despite the apparent abundance of material, few studies are devoted to spinel from xenoliths in kimberlites. For example, in the largest study of spinel from different parageneses [6], only 409 analyses from 26,297 belong to mantle and lower-crust xenoliths from kimberlites. This is probably due to a relatively small number of samples (compared, say, with xenoliths from basalts or ophiolites) available to researchers. Such xenoliths, as a rule, are spinel- and garnet-spinel lherzolites.

At the same time, an extremely rare group of the most depleted mantle rocks exists—megacrystalline peridotites, represented by harzburgite–dunite. Megacrystalline harzburgite–dunites (MHD) have been encountered in individual kimberlite pipes, mainly Udachnaya pipe (Yakutia). These unusual rocks with incompletely replaced olivine were first discovered in 1977 [7]. The rocks are composed of nearly pure olivine (90% or more)—normally it is one megacrystal and sometimes, but rarely, 2–3 megacrystals. Less than 10% of the rock makes up a Cr-pyrope garnet and/or enstatite and/or Cr-spinel. MHD rocks are one of the parental rocks of Siberian diamonds [7–11]. The chemical composition of the minerals is identical to that of mineral inclusions in diamonds [11] (and references therein) [12]. The high concentration of Cr_2O_3 in olivine, the low $Fe^{3+}/(Fe^{3+} + Cr + Al)$ in chromite, low contents of TiO_2 and CaO in pyrope, and the presence of diamond in mineral parageneses provide

evidence for reduced conditions during the formation of these rocks and their low metasomatic alteration [13,14]. Oxygen fugacity evaluations for this group of mantle peridotites obtained by two independent methods—electrochemical cells and gas chromatography—showed that although the highest number of values is located in the region of the buffer equilibrium wuestite–magnetite (WM), a significant variance in the values between the quartz–fayalite–magnetite (QFM) and iron–wuestite (IW) buffers is observed [15–18]. A wide range of redox conditions, resulting in the formation of the rims around garnet and coexistence of several spinel generations in some MHD, suggest that some part of the rocks have been subjected to metasomatic effects before being brought to the surface by kimberlite. This study focuses on such rocks.

In megacrystalline dunites (olivine + garnet; olivine + garnet + spinel; olivine + spinel) and harzburgites (olivine + garnet + orthopyroxene; olivine + garnet + orthopyroxene + spinel; olivine + orthopyroxene + spinel), spinel is present among the rock-forming and accessory minerals, as inclusions in other phases as well as a mineral in the rims around garnet [19], showing, as a rule, that it is zoning "core-edge"-type. The study of the chemical composition of various kinds of spinel from MHD allows for evaluation of the nature and extent of the alteration process that occurred in the most depleted part of the lithospheric mantle before and during the involvement of the rocks in kimberlite explosion.

Some aspects of this article were partially reported at international conferences in Morocco [20] and Russia [21]. In the study presented here, I try to look at the problem more broadly and, taking as my starting point a set of spinel generations from the most depleted mantle rocks, to trace the general tendencies of transformation of the mantle spinel compositions of different parageneses.

2. Methods and Samples

The chemical compositions of minerals were determined with a scanning electron microscope (SEM) MIRA3 LMU (TESCAN, Brno, Czech Republic) at an accelerating voltage of 20 kV and a counting time of 20 s and an electron probe microanalyzer (EPMA) JXA-8100 (JEOL, Tokyo, Japan), using an acceleration voltage of 20 kV, a focused beam with a current of 10 nA, counting times of 20–30 s, and standard PAP correction procedures [22,23]. Precision and accuracy were monitored using natural and synthetic standards that were measured at regular intervals during each analytical session. Detection limits are typically <0.04 wt.% for SiO_2, TiO_2, Al_2O_3, MgO, CaO, Na_2O, and K_2O, <0.05–0.07 wt.% for FeO, MnO and Cr_2O_3. The values of microimpurities (CaO, Na_2O, Al_2O_3, Cr_2O_3) in olivine, necessary for the calculation of P-T parameters, were determined using a technique described in [24]. In order to work on the devices, flat polished sample slabs with carbon coating were used.

Thirty-six typical MHD are investigated in the course of the work. Samples are nodules from kimberlite measuring 2 to 8 cm in diameter, consisting mainly of transparent greenish olivine (single, sometimes cracked, crystals). A general view of the rocks is presented in Figure 1a–c. Eleven of them contain primary Cr-spinel (six samples—Cr-spinel only (Figure 1d), five samples—Cr-spinel and Cr-pyrope (Figure 1e)). Twenty-five samples contain pyrope only. All of them have thin keliphitic rims situated around the garnet (Figure 1f). In some samples the microcracks in olivine are filled with secondary minerals (the evidence of later effects on the rocks), including zoned spinel. One dunite is distinguished by chromite inclusions within rounded sulfide inclusions in olivine.

After Roeder [25], I use the term "spinel", which encompasses the whole spinel group (spinel—written with a lowercase letter), and only rarely implying the $MgAl_2O_4$ end-member (Spinel—written with a capital letter).
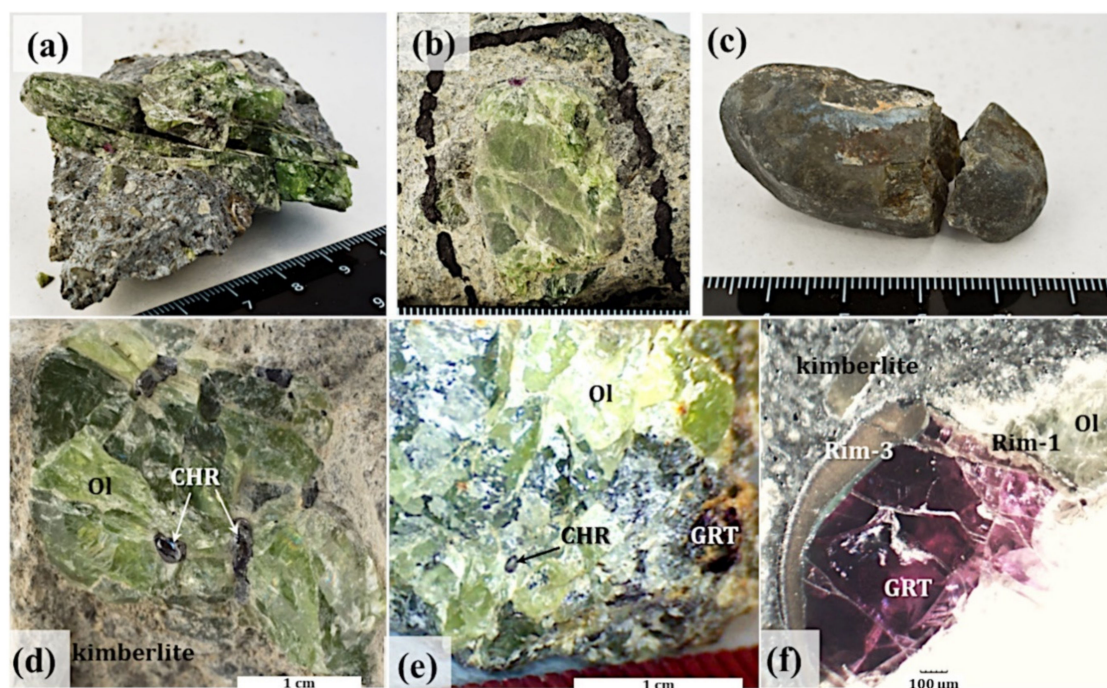
Figure 1. Megacrystalline harzburgite–dunites (MHD) from Udachnaya pipe, Yakutia, represented as follows: (**a**–**c**) general view of the rocks: (**a**,**b**) xenoliths in kimberlite; in **b**, the black line outlines xenolith in kimberlite; (**c**) extracted nodule; in **a**–**c**, fine divisions on the ruler are mm; (**d**) olivine (Ol) and Cr-spinel (CHR); (**e**) olivine (Ol), pyrope garnet (GRT) and Cr-spinel (CHR); (**f**) olivine (Ol) and pyrope garnet (GRT) with kelyphitic rims (see text for description of the rims).

The following kinds of spinel occur in the studied xenoliths:

(1) Primary Cr-spinel (Cr/(Cr + Al) = 80%–90%) with the typical zoning "core-edge" and magnetite rim (Figure 1d,e and Figure 2a).

(2) Spinel from the kelyphitic rims around pyrope [19]: Rim1 (Al-orthopyroxene + spinel ± phlogopite ± Al-clinopyroxene ± amphibole ± sodalite, calcite, potash feldspar, magnetite and sulfides, including djerfisherite) between garnet and olivine, but closer to garnet; Rim2 (phlogopite border of the Rim1 ± Al-orthopyroxene, spinel, and Al-clinopyroxene) between garnet and olivine, but closer to olivine; Rim3 (phlogopite + spinel + magnetite) between garnet and kimberlite (Figures 1f and 2c,d).

(3) Inclusions of spinel in pentlandite, bordered with djerfisherite. The sulfides are observed in randomly throughout of olivine in megacrystalline dunite. The spinel inclusions are present in the central and marginal parts of sulfides (Figure 2e,f).

(4) Spinel with a wide range of compositions from olivine microcracks, filled by low-iron serpentine in association with calcite, apatite, ilmenite, high-magnesia Ba-containing phlogopite, magnetite, perovskite, and sulfides (Figure 2b).

This paper also contains analytical results from previous studies of mantle xenoliths from the Udachnaya kimberlite pipe published over a range of years [17,19].
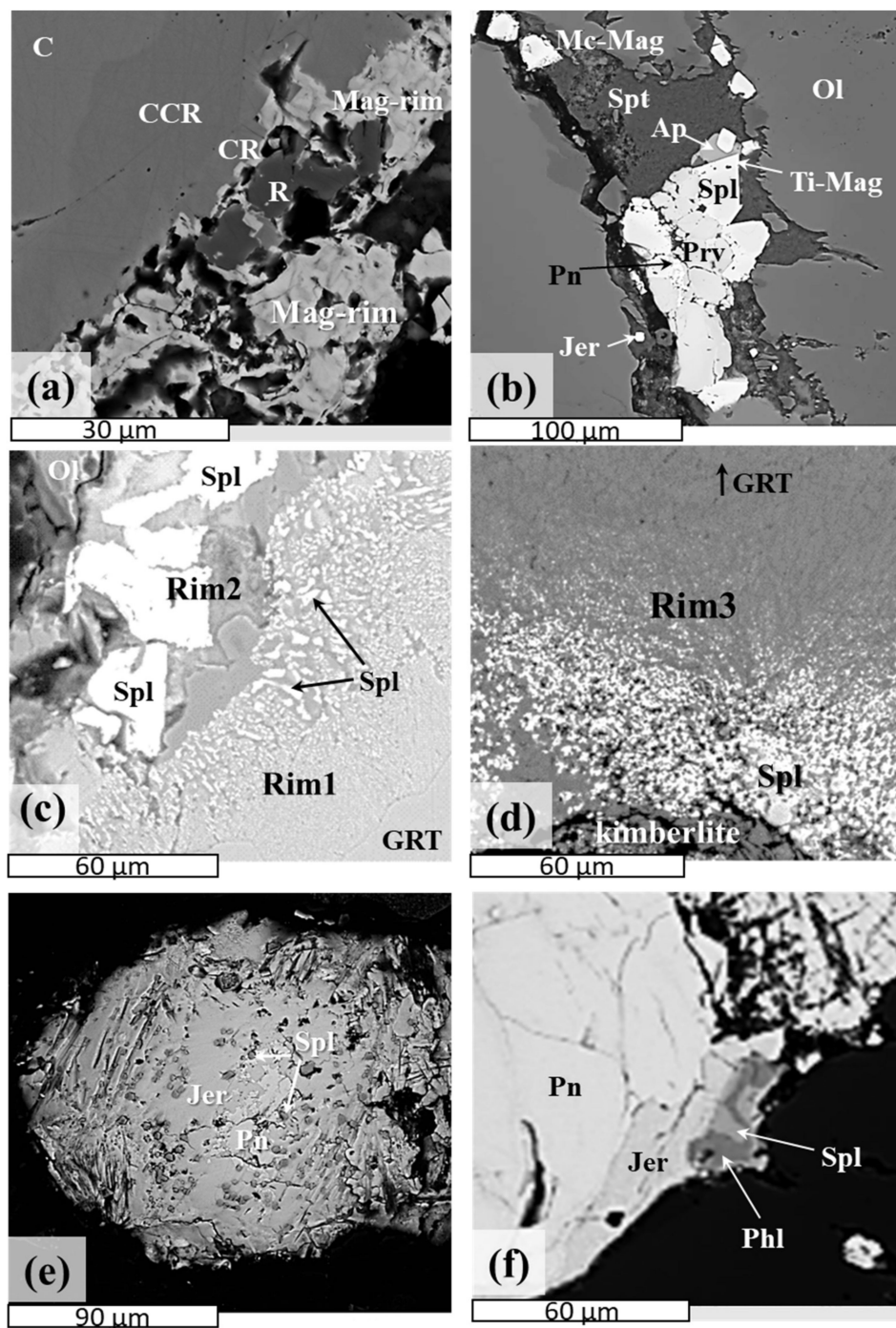
Figure 2. Spinel species from MHD (Udachnaya pipe, Yakutia), BSE images: (**a**) zoned primary Cr-spinel with Cr_2O_3 content, wt.%, from core to edge C (63.7), CCR (49.5), CR (24.4), R (1.42), Mag-rim (1.00) given in Table 1; (**b**) spinel in association with apatite, perovskite, Ti-magnetite, sulfides (pentlandite and djerfisherite) in olivine microcracks filled with serpentine; (**c**) spinel from the kelyphitic rims (Rim1 and Rim2) around garnet (boundary "garnet–olivine"); (**d**) spinel from the Rim3 around garnet (boundary "garnet–kimberlite"); (**e**) spinel inclusion in sulfide core; (**f**) spinel inclusion in association with phlogopite in sulfide edge. Ap—apatite; GRT—garnet; Jer—djerfisherite; Ol—olivine; Pn—pentlandite; Prv—perovskite; Phl—phlogopite; Spt—serpentine; Spl—spinel; Ti-mag—Ti-magnetite.

Table 1. Representative compositions of spinel species from MHD (Udachnaya pipe, Yakutia), this study, SEM and EPMA*.

Sample	2/09 *	49/10 *	164/09 *	43/01 *	588/11 *	180/10	180/10	180/10	180/10	180/10
	C	C	C	C	C	C	CCR	CR	R	Mag-rim
TiO_2	0.25	0.08	0.11	0.36	0.11	0.92	4.46	13.4	22.24	3.55
Al_2O_3	5.06	5.64	8.02	4.13	4.89	5.21	8.03	6.94	6.27	0.00
Cr_2O_3	65.1	65.78	63.2	64.2	65.3	63.7	49.5	24.4	1.42	1.00
FeO tot	18.1	16.46	15.4	17.2	18.0	19.8	26.7	42.2	51.6	93.1
MnO	0.27	0.212	0.24	0.28	0.28	0.00	0.00	0.00	1.86	1.33
MgO	11.5	12.21	13.0	11.9	11.4	10.4	11.1	13.1	16.62	1.0
Total	100.0	100.4	99.9	98.1	100.0	100.0	99.7	100.0	100.0	100.0
Fe^{3+}/Fe^{2+}	0.19	0.16	0.16	0.25	0.19	0.14	0.50	1.42	3.00	1.96
$Cr/(Cr + Al)$	89.61	88.67	84.10	91.26	89.96	89.13	80.51	70.22	13.19	100.0
$Fe^{2+}/(Fe^{2+} + Mg)$	0.43	0.40	0.36	0.39	0.43	0.48	0.47	0.43	0.30	0.95
$Fe^{3+}/(Fe^{3+} + Al + Cr)$	0.04	0.03	0.03	0.05	0.04	0.04	0.13	0.43	0.79	0.98
Sample	avg 21 *	avg 15 *	avg 24 *	702/13	702/13	702/13	702/13	702/13	702/13	702/13
	Rim1	Rim2-C	Rim2-E	Rim3-C	Rim3-E	Su-C	Su-E	Mc-C	Mc-E	Mc-Mag
TiO_2	0.38	3.38	0.52	7.24	4.64	0.44	9.05	5.46	12.72	3.58
Al_2O_3	37.95	12.12	32.62	4.37	0.66	0.00	5.15	5.08	2.78	0.00
Cr_2O_3	27.38	46.52	32.08	19.94	11.72	64.08	34.04	50.67	1.3	0.00
FeO tot	14.79	23.43	16.17	57.28	75.61	23.52	41.7	27.18	72.45	91.15
MnO	0.37	0.48	0.39	1.71	1.58	0.00	1.42	0.00	1.69	0.6
MgO	17.69	12.39	16.47	9.06	5.42	10.48	7.78	11.42	8.65	4.27
Total	98.56	98.31	98.24	99.60	99.63	98.52	99.14	99.81	99.59	99.60
Fe^{3+}/Fe^{2+}	0.43	0.54	0.43	1.89	2.09	0.48	0.87	0.59	2.28	2.37
$Cr/(Cr + Al)$	0.33	0.72	0.40	0.75	0.92	1.00	0.82	0.87	0.24	0.00
$Fe^{2+}/(Fe^{2+} + Mg)$	0.25	0.41	0.28	0.55	0.72	0.46	0.62	0.46	0.59	0.78
$Fe^{3+}/(Fe^{3+} + Al + Cr)$	0.05	0.12	0.06	0.60	0.81	0.11	0.33	0.15	0.91	1.00

C—core; E—edge; C–CCR–CR–R–Mag-rim—composition change of primary chromite from core to Mag-rim in edge; avg—average; Su—inclusion in sulfide; Mc—Spl in microcracks of olivine. The types of spinel from the Table can be seen in Figure 2.

3. Results

3.1. Spinel Compositions

From the above-mentioned varieties of spinel, in world literature chemical compositions were previously published only for the primary (rock-forming) Cr-spinel of depleted peridotites from kimberlites ([9,11,12]—MHD, Yakutia; [26] and references therein—harzburgite, Africa). In this paper, an attempt is made to track changes in the composition of various parts of the spinel grains of all the generations found and the basic ratios of the main components, from which one can judge the conditions for the formation of a particular spinel (Table 1, all numbers of samples in the Table begin with LUV).

The ratio $Cr/(Cr + Al)$ reflects the degree of depletion and/or the depth of formation of the rock, and Fe^{3+}/Fe^{2+} (or mole fraction Fe_3O_4) is an indicator of the redox conditions [6,25,27–30].

Figure 3a shows good inverse correlation Cr#-Fe^{3+}/Fe^{2+} observed in the primary chromite when moving from the grain core to the edge (see also Table 1, LUV180/10 C–R). Figure 3c shows good direct correlation as well during the formation of a non-aluminous magnetite rim containing 1 wt.% Cr_2O_3 (Table 1, LUV180/10 CR–Mag-rim).

Spinel from Rim1 and Rim2 is the product of the reactionary replacement of the garnet-host; therefore, the content of chromium and other components in it, in addition to the depth of formation, must be determined by the amount of such components in the primary pyrope (degree of depletion). The central part of the spinel from Rim2 has a composition close to the composition of the intermediate zone CCR of the primary chromite (Figure 2a), the edge of the spinel from Rim2 is similar in composition to the spinel of Rim1 (Figure 3c). In Figure 3a,b, one can observe a sharp decrease in the Cr component in the spinel from Rim2 to Rim1 up to the chromium content in the host pyrope. The ratio of Fe^{3+}/Fe^{2+}, in this case, varies less significantly. In spinel of Rim3 from the core to the edge, an increase in the magnetite molecule occurs simultaneously with an increase in the $Cr/(Cr + Al)$ ratio (Figure 3c). Spinel from the central part of sulfide is practically pure chromite, while inclusions of spinel in the marginal parts of sulfide grains contain alumina in their composition and a greater amount of oxidized

iron (Figure 3b,c, Table 1, LUV702/13, Su-C—Su-E). The most pronounced zonation "core-edge" was observed in spinel from microcracks in olivine, where a sharp decrease in chromium content was accompanied by a significant increase in ferric iron. A small grain of practically pure magnetite was found in another microcrack (Figure 3c, Table 1, 702/13, Mc-Mag). This composition is identical to the composition of the magnetite rim around the primary chromite with the difference that there is no admixture of chromium here.

Figure 3. Diagram Cr/(Cr + Al)-Fe^{3+}/Fe^{2+} for spinel species from MHD (Udachnaya pipe, Yakutia): Primary—primary Cr-spinel; C–CCR–CR–R–Mag-rim—composition change of primary chromite from core to Mag-rim in edge (see also Table 1, Figure 2a); Rim1,2,3—spinel from kelyphitic rims around garnet; grt—rock-forming Cr-pyrope (see comments in text); Su—spinel inclusion in the center and marginal parts of sulfide; Mc—spinel from the microcracks in olivine; arrows indicate core-edge direction; R^2—correlation coefficient for (**a**) and (**b**). (**a**) megacrystalline peridotites LUV180/10 and LUV49/10, containing both Cr-spinel and Cr-pyrope; (**b**) megacrystalline peridotites LUV159/10-2 and LUV702/13, containing Cr-pyrope and sulfide; (**c**) united general scheme for all spinel species.

It is necessary to emphasize one interesting regularity—all magnetites forming the edges of spinel species (Table 1) contain about 1.5 wt.% MnO, which is not inherent in mantle spinels from xenoliths of Yakutian kimberlites.

3.2. Spinel Thermometry and Barometry

This paper does not delve into the thermobarometry of depleted peridotites, but some comments are necessary. Equilibrium P-T estimates are difficult, primarily due to the absence of pyroxenes in the paragenesis (enstatite occurs in rare samples). Temperatures for MHD rocks have been determined using Mg-Fe ratios in olivine and garnet [31] with pressure from alumina isopleths in enstatite (if present) that is in equilibrium with garnet [32]. Thermometers and barometers based on microimpurities in garnet or olivine [33–36] cannot be accurately applied with a standard microprobe analysis. As petrologists and experimenters previously proposed [11,37,38], the Cr–Ca ratio in pyrope can be used as a barometer for lherzolites and harzburgites (formulated in [39]).

The geothermometer based on the partitioning of Al_2O_3 between forsterite-rich olivine and Cr-rich spinel [40] is of interest in this study. This thermometer has some limitations (Fe^{3+} < 0.1, Ti < 0.025 in spinel) and requires the use of exact values for Al_2O_3 in olivine. Figure 4a shows that the temperature estimates obtained using this experimental thermometer are slightly higher than those calculated from garnet–olivine [31] and monomineral olivine [36] thermometers, but are generally commensurable with the latter. Such a small discrepancy could be caused by the increased Cr# of primary Cr-spinel from MHD (0.70–0.91) compared to those participating in the experiment (0.07–0.69). Pressures from the olivine barometer [33] agree well with the monomineral garnet barometer of [39] (Figure 4b). Points of P-T-condition estimates for MHD, calculated by rock-forming olivine and Cr-spinel, lie in the field of diamond stability slightly lower the heatflow geotherm 40 mwm^{-2} (Figure 4c). Data for seven megacrystalline harzburgites, taken from [11], calculated using the thermometer [31] and the barometer [32] (indicated by bricks in Figure 4c) show lower P-T parameters and plot closer to the mantle heatflow geotherm 35 mwm^{-2}. As was shown in [11], four studied samples contained Cr-spinel; therefore, it was logical to determine their temperature and pressure using a thermobarometer, which is also used here for MHD (Figure 4c, a field surrounded by a solid line). The result was highly overestimated, most likely due to the use of inaccurate values of trace impurities (Al_2O_3 and CaO) in olivine, obtained using standard microprobe analysis of that time.

P-T estimation for spinels in Rim1,2 was attempted. By chemical composition, some of them fit well in the limited range of the thermometer [40]. However, calculating the temperature requires equilibrium olivine, which does not occur in the rims. Rock-forming olivine was used. It shows zoning with Al_2O_3 and CaO increasing toward garnet, 1.2–1.8 times higher than in the grain core. Concentrations increase by several times near microcracks. Since Rim1 is closer to the garnet, olivine, which is located closest to garnet (with maximum Al_2O_3 and CaO), was paired with spinel from this Rim. Points lie in the graphite stability field above heatflow geotherm 40 mwm^{-2} (Figure 4c). To calculate the P-T of Rim2 (located closer to the olivine), Al_2O_3 and CaO of the olivine parts that were located far from the garnet (as in the case of the primary chromite) were used along with the components of the spinel from this Rim. Estimates for couples "olivine–spinel of Rim2" are located near the geotherm 40 mwm^{-2} and the graphite–diamond line in the field of graphite stability (Figure 4c). Unfortunately, the compositions of spinel from microcracks and inclusions in sulfide did not fit into the composition range suitable for the thermometer [40]; P-T estimates could not be made even approximately.
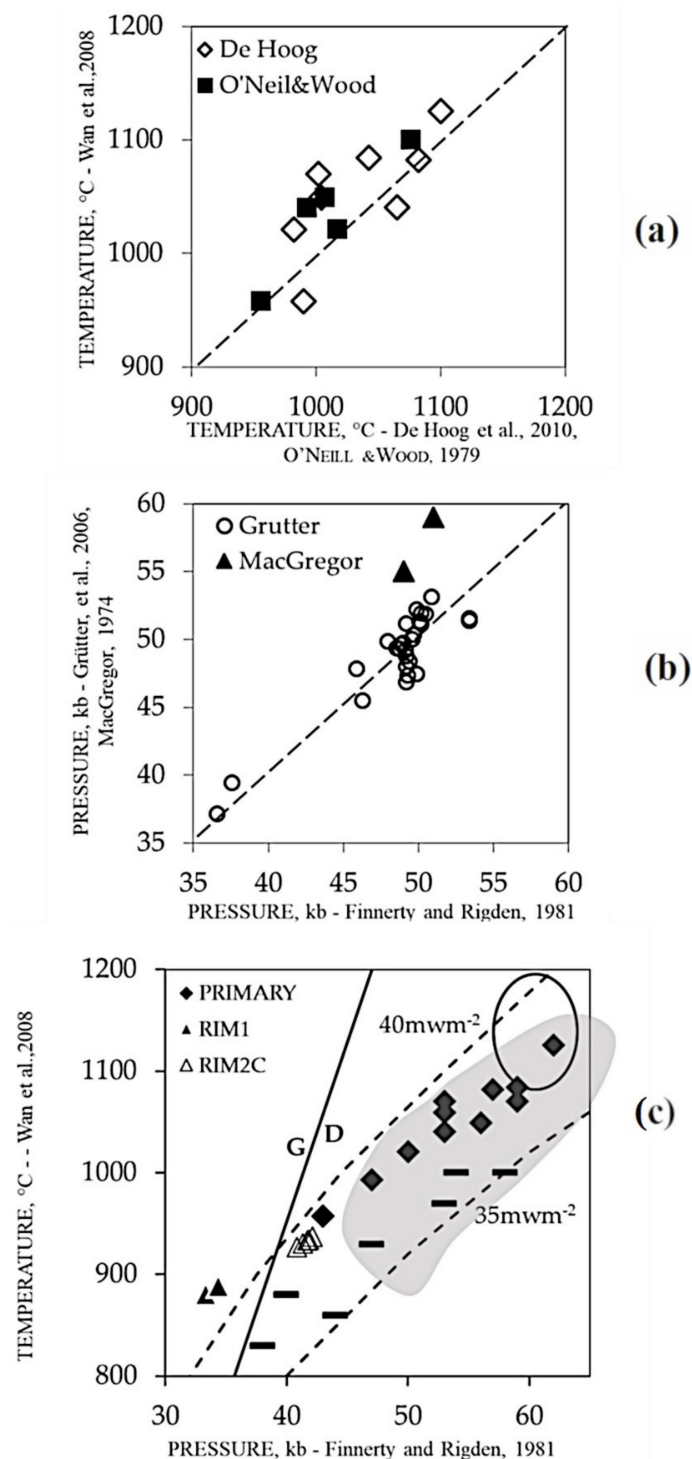
Figure 4. (**a**–**c**) Thermobarometry of Cr-spinel-bearing MHD (Udachnaya pipe, Yakutia). (**a**) temperature estimates by [40] against temperature calculated using [31] and [36] thermometers; (**b**) pressure estimated using [39] and [32] against pressure calculated using [33] barometer. See comments in the text for (**a**) and (**b**). (**c**) P-T-estimates for Cr-spinel-bearing MHD from Udachnaya pipe: Primary—primary Cr-spinel; Rim1,2—spinel from kelyphitic rims around garnet. The solid line separates the stability fields of graphite and diamond [41]; dotted line—mantle heatflow geoterms 40 and 35 mwm^{-2} [42]. Data of the previous studies: Rectangles—megacrystalline harzburgites from Udachnaya pipe, Yakutia [11], grey field—low Ca harzburgites from Daldyn field, Yakutia [34], enclosed oval field—explanations in the text.

4. Discussion

Studying the variations of the chemical composition of different spinel generations from MHD in comparison with spinels from all possible mantle parageneses offers a chance to track the complex transformations of rocks occurring from the moment of their formation to being brought to the surface by kimberlite and to identify the processes responsible for these changes.

The different types of spinels, which are sometimes present in the same sample, vary significantly in terms of their component composition, and practically all are zoned indicating multi-stage, non-simultaneous formation.

The compositions of the studied samples are plotted on the compositional triangle Spl ((Mg,Fe)Al_2O_4)–Chr ((Mg,Fe)Cr_2O_4)–Mag ((Mg,Fe)$Fe^{3+}_2O_4$) (Figure 5). Two trends in the composition change of the studied spinels are clearly visible—from Chromite to Spinel and from Chromite to Magnetite. Another trend, not shown in [6] (from Spinel to Magnetite across the Spinel Gap), is traced for spinels from garnet alteration zones in eclogites of groups A, B, C from the Udachnaya pipe (Figure 5: Brown field).

The spinels from Rim1,2 fit well on the Cr–Al trend, which was first described by Irving [2] as a positive correlation of the Cr/(Cr + Al) and Fe^{2+}/(Fe^{2+} + Mg) ratios (see Table 1) in the equilibrium of spinel with an olivine of constant composition at constant T. For high-pressure samples, these were probably the result of equilibria between Al-bearing pyroxenes and Mg-Al-rich spinel [6], which was observed in our case, considering the mineral association of Rim1,2 (see the description of the samples in Section 2). The spinel compositions of peridotitic mantle parageneses are located along this direction (Figure 5a, color fields: Orange, pink, blue, and ocean green). The point of composition of the central part of primary spinel grain from MHD lies in the field of spinel inclusions in diamonds. The final composition of this trend, which does not contain alumina, is represented by chromite inclusion in the central part of sulfide. The increase in Fe^{3+} is marked as a kimberlite trend and is similar to Fe–Ti trend (Figure 5a). In our case, these trends are represented by the gradual formation of a rim on the primary rock-forming spinel, a rim on spinel from microcracks in olivine, and the formation of Rim3 around the garnet. The Fe–Ti trend is typically characterized by simultaneous increases in Fe^{2+} and Fe^{3+}, with titanium increases in spinel due to fractional crystallization of silicates from the host magma [6]. The TiO_2 contents of mantle spinels, as a rule, are low (0.5 wt.%) and correlate with the level of xenolith depletion. Some sectors of spinel species from MHD demonstrate compositions with an enriched Ti content (Table 1).

In contrast to the overwhelming majority of terrestrial spinel from the various environments and localizations presented in [6], titanium enrichment of spinel species from MHD occurs in the postcrystallization period and occurs in multiple stages. Moreover, if at the early stages (ancient metasomatism), a smooth increase in the Ti component occurs in later generations, then, under the influence of a kimberlite melt, titanium often forms its own phase (ulvospinel, perovskite, ilmenite), and an increase in Fe^{2+} and Fe^{3+} leads to the formation of low-Ti magnetite at the very last stages of spinel transformation. This is evident in the formation of the rim of the primary rock-forming spinel, in which essentially, simultaneous formation of a phase with a very high percentage of ilmenite (R in Figure 2a and Table 1, LUV180) and magnetite with a low-Ti concentration (Mag-rim in Figure 2a and Table 1, LUV180) occurs.

As can be seen from Table 1, the outer part of primary Cr-spinel (Mag-rim) and the spinel from the microcrack (Mc-Mag) are essentially pure magnetite, indicating the highly oxidizing nature of the environment. The very high content of FeO-tot is also found in the edges of spinel from microcracks (Mc-E) and Rim3 (Rim3-E): 72.45 wt.% and 75.61 wt.%, respectively. However, in the composition of spinel Mc-Mag from microcrack, along with the high Fe^{3+}/Fe^{2+}, Cr and Al are absent, and the Cr/(Cr + Al) ratio becomes meaningless, whereas in the primary Cr-spinel and Rim3-spinel, the Cr#-ratio increases with increasing Fe^{3+}/Fe^{2+} (Figure 3c). Evidently, this increase in Cr# cannot be caused by an increase in depth or depletion of the system during Rim3 formation or magnetite rim

growth around the primary Cr-spinel. Most likely, Rim1 is converted to Rim3 under the influence of the kimberlite melt, which carries the rock to the surface.
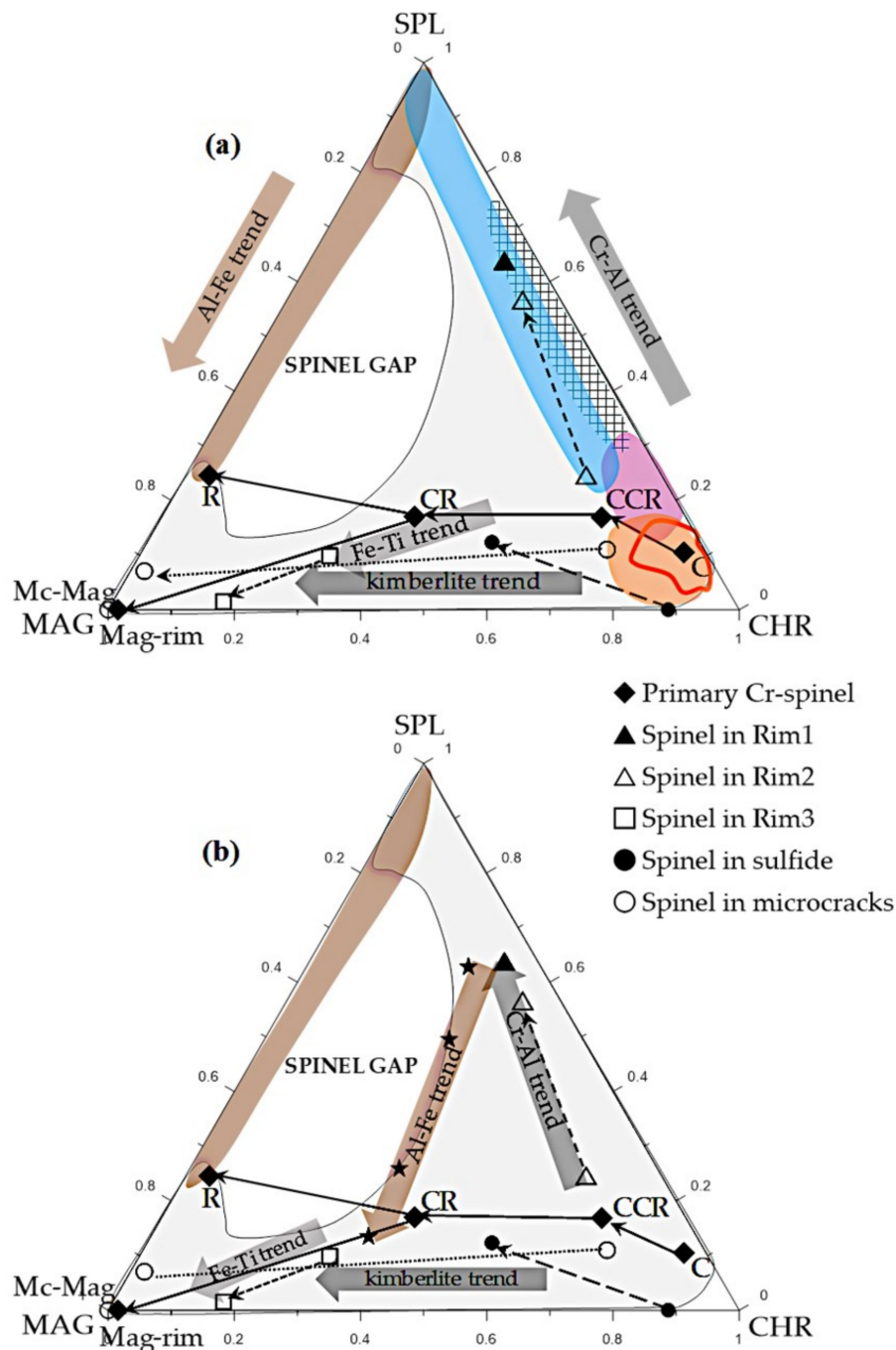

Figure 5. Spinel (SPL)–Chromite (CHR)–Magnetite (MAG) compositional triangle. The gray field of the terrestrial spinel dataset is composed of 21,644 analyses and spinel inclusions in diamonds (field contoured by orange line) taken from [6]. C–CCR–CR–R–Mag-rim—composition change of primary chromite from core to Mag-rim in edge. Thin black arrows indicate core-edge direction. Color fields on (**a**): Orange—MHD; pink—garnet–spinel lherzolites [17]; ocean green net—spinel lherzolites [17]; blue—garnet rims of deformed lherzolites [19]. Color fields on (**a,b**): Brown—rims and zones of garnet alteration from eclogites [19]. Three main trends [6], reflecting the variable relationships between the components of spinel composition, are shown by thick grey arrows on (**a,b**): Cr–Al, kimberlite, Fe–Ti. The thick brown arrow shows an Al–Fe trend from this study. The stars on (**b**)—intermediate spinel compositions (see the text for details).

The kimberlite melt, upon interaction with the captured rock, produces a large amount of K and water. The silicate minerals of Rim1 are replaced by phlogopite ($KMg_3(Si_3Al)O_{10}(OH)_2$),which is the main mineral of Rim3. Aluminous spinel from Rim1 in the enriched system under the influence of increasing oxygen potential is almost completely replaced by spinel with a very high magnetite component and a small Cr_2O_3 content. However, since most Al is positioned in the phlogopite, the Cr# ratio in spinel shows growth. A similar "arithmetic trick" takes place for the marginal part of the primary spinel, where, along with the formation of magnetite (Table 1, LUV180, CR → Mag-rim), a spinel with a high titanium content is also formed (Figure 2a, R), "capturing" a small amount of aluminum that was present in the grain before its change (Table 1, LUV180, CR → R).

For a long time, there was no material evidence of the formation of Rim3 from Rim1 as a result of the capture of rock by kimberlite magma. However, recently a spinel of intermediate compositions was found in the Rim around a garnet of one of the megacrystalline peridotites (Figure 5b: Stars from Rim1 to Rim3), which supports the model detailing the conversion of Rim1 to Rim3. The rarity of the occurrence of such compositions is apparently due to the very short period in which the conditions for their formation exist and the rapid rebalancing of the compositions. The chain of spinel compositions (denoted by stars in Figure 5b) from Rim1 to Rim3 from MHD coincides with the Al–Fe trend of spinels from rims of eclogite garnets. This result suggests a single process of reworking the mantle material with the oxidized fluids before capturing the rocks by kimberlite.

To understand the sequence of processes responsible for changes in the composition of spinel species from MHD, taking into account the role of Ti, I recalculated the spinel compositions into four independent extreme terms, separating Al, Cr, Fe^{3+}, Ti: Spinel–$(Mg,Fe^{2+})Al_2O_4$; Chromite–$(Mg,Fe^{2+})Cr_2O_4$; Ferrite (magnetite)–$(Mg,Fe^{2+},Mn)Fe^{3+}_2O_4$; Ilmenite–$(Mg,Fe^{2+})TiO_3$ (Figure 6).

Cr–spinel included in the central part of the sulfide demonstrates the highest proportion of the Chromite component (88%) (Figure 6d, black line). A similar composition has a rock-forming Cr–spinel core (Figure 6a, black line) (85% of the Chromite component). However, the relation $Fe^{3+}/(Fe^{3+}+Al + Cr)$ showing the degree to which a system is oxidized (for example, [13]) is much lower for rock-forming Cr–spinel (0.04) in comparison with Cr–spinel in the sulfide core (0.11) (Table 1). This is due to different impurities in these spinels. In spinel inclusion in sulfide 11% is Ferrite, while for the core of primary Cr–spinel, the second most significant component (10%) is Spinel. Nevertheless, the Cr–spinel inclusion in the core of sulfide represents one of the earliest species of the spinel set under investigation, since sulfide inclusions are apparently syngenetic with olivine-host. Both spinels do not contain the Ilmenite component, since they were not directly affected by the metasomatic fluid and the kimberlite melt.

Spinel in microcracks (Figure 6b, red line) looks like primary Cr-spinel of the later generation (Figure 6a, CCR composition, red line), as can be evidenced by the high chromium content in the center of the grain and small grain sizes. Small spinel inclusions in olivine were those weakened areas through which the cracks passed in the period preceding the capture of the rock by kimberlite melt. It is probable that during the growth (or transformation by re-equilibration of the composition) of this spinel, the rock was exposed to hot deep metasomatic melts/liquids, which brought a significant amount of Ti and Fe (more than 10% of Ilmenite and Ferrite components occur in CCR-primary Cr-spinel and core of Cr-spinel in olivine microcracks). This process is connected with the early stages of lithospheric mantle evolution and was caused by ancient metasomatism [43,44], which is responsible for increasing titanium, calcium, and iron in the outer parts of peridotite garnets [43–45] and an increase in the iron content of olivine near cracks. Probably at the same time, or shortly after, Rim2 around the garnet began to form (Rim2-C: Figure 6e, red line). Continued enrichment of Ti and Fe led to a further change in the composition of the marginal part of the primary spinel (Figure 6a, CR composition, green line) and the transformation of the composition of spinel inclusions located on a sulfide surface (Figure 6d, grey line).
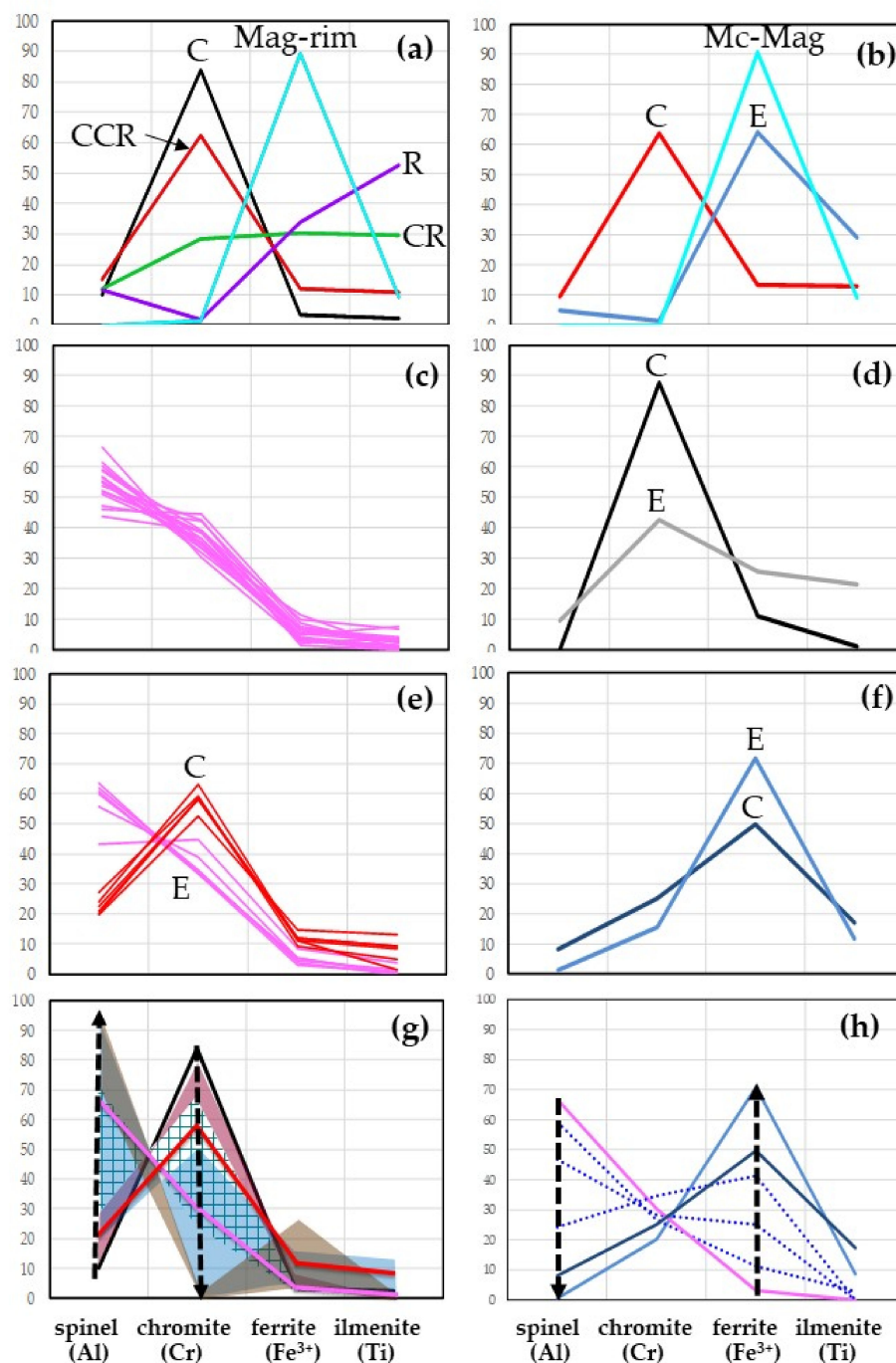
Figure 6. Extreme members of spinel species of MHD from Udachnaya pipe: (**a**) primary Cr-spinel from LUV180/10, (**b**) spinel from the microcracks of olivine, (**c**) spinel from Rim1, (**d**) spinel inclusions in sulfide from LUV702/13, (**e**) spinel from Rim2, (**f**) spinel from Rim3. Zones of the spinel species are given according to Table 1. C—core, E—edge. Spinel compositions of other mantle parageneses are presented in (**g**): Fields of rock-forming spinel from spinel-garnet lherzolites [17]—pink; spinel lherzolites [17]—ocean green net. Fields of the spinel of Rims around garnet from deformed lherzolites [19]—blue; eclogites [19]—brown. For comparison, lines of the primary spinel and spinel of Rim2 and Rim1 from MHD are given. (**h**) Rim3 of garnet from peridotitic parageneses—blue lines; intermediate spinels marked with stars in Figure 5b—bright blue dotted lines. Note: Lines of the same color show the same and similar compositions.

Subsequently, the metasomatism activity appeared to weaken for some time, the temperature of the system decreased, and the Cr/(Cr + Al) ratio began to shift towards Al, following the Cr–Al trend (Figure 5). This led to the formation of Rim1 spinel and edges of Rim2 spinel (Figure 4c) with a predominance of the Spinel (Al) component (Figure 6c,e, rose lines). Therefore, the formation of rims (Rim1 and Rim2) around the MHD garnets, which do not contact with kimberlite, occurred before the xenoliths were captured by the kimberlite melt, as confirmed by $^{40}Ar/^{39}Ar$ dating of these rims [46]. The P-T formation parameters of spinel from Rim1–2 (Figure 4c) coincide with those for spinel lherzolites [17], and the lines reflecting their component composition practically contour the field of spinel lherzolites (Figure 6g, red is average for Rim2-C, pink is average for Rim1). The only difference is the presence of the Ilmenite component (Ti) in the Rim2-C spinel and its complete absence in spinel from spinel lherzolites. The presence of Ti in the spinel from Rim2-C is probably due to the process described above—the ancient metasomatic enrichment of the outer parts of the grains of peridotite garnet, from which Rim2 were subsequently formed. Such enrichment has mostly affected the garnets from deformed lherzolites, and it is in the spinels from the rims around them that the highest Ti content is observed (Figure 6g, blue field).

Figure 6g clearly shows a consistent change in the composition of spinels following the Cr–Al trend from the central part of the primary Cr-spinel of the most depleted mantle rocks—MHD—to the spinel in kelyphitic rim of the most enriched—deformed lherzolites. This change is expressed mainly in the increase in the Spinel component and the decrease in the Chromite component (black dashed arrows) in the series of parageneses: MHD → garnet-spinel lherzolite → spinel lherzolite (+Rim2-C-MHD) → spinel lherzolite + deformed lherzolite (+ Rim1-MHD) → deformed lherzolite.

Kimberlite formation and the activation of kimberlite fluids and melts with subsequent capture of xenoliths during eruption were accompanied by changes in the composition of spinel, characterized by a sharp increase in the role of oxidized iron. At this time, a magnetite/ulvospinel edge on a primary spinel (Figure 6a, cyan and blue purple lines), as well as a magnetite rim on a spinel from microcracks in olivine (Figure 6b, blue and cyan lines) were formed. In the composition of these spinels, Chromite (Cr) was unquestionably the predominant component (Figure 6a,b); therefore, the increase in the Ferrite (Fe^{3+}) component to a maximum in the outer part occurs following the kimberlite and Fe–Ti trends. At the same time, Rim1 (Figure 6h, pink line) was converted step by step through intermediate compounds (Figure 6h, bright blue dotted lines) to Rim3 (Figure 6f, dark blue and blue lines). The Spinel component dominated in the spinel of Rim1. Therefore, there is a sharp increase in the Ferrite component (Fe^{3+}) with the reduction of the Spinel (Al) to zero (Figure 6g, black arrows), while the Chromite (Cr) and Ilmenite (Ti) components do not play a significant role at this stage. A change in the composition occurs along the Al–Fe trend of eclogite spinels (Figures 5 and 6g, brown field). The compositions of spinel in Rim3 for peridotite rocks of contrasting parageneses—ultra-depleted MHD and ultra-enriched deformed lherzolites—are completely identical (Figure 6f,h, blue lines) as they are the result of the transformation, with further re-equilibration, of the Rim1 → Rim3 compositions under the influence of the same kimberlite melt.

5. Conclusions

The complexity of this study was that it was necessary to draw conclusions, simulate the processes, and build a sequence of spinel generations, based only on a detailed analysis of its composition and morphology. For natural reasons (limiting the volume of the article, focusing on a certain mineral, etc.), spinel was considered mainly in isolation from paragenesis, of which it is a part. The relationship with the silicate phases (except for one mention of phlogopite, which forms in the rim around the garnet and the use of the olivine composition in the calculation of P-T conditions) was not considered. However, such an approach made it possible to reveal important stages of the mantle composition transformation, the indicator of which was spinel composition. As a result, it was possible to establish the following:

1. In the depleted mantle, sulfides are formed under strongly reducing conditions; however, as the comparison of the $Fe^{3+}\#$ ratio in chromite from the central part of sulfide and in the core of primary chromite from MHD shows, the latter is formed in an even more reduced environment.

2. The enrichment of the depleted mantle rocks by Ti and Fe occurred more than once. The stages of enrichment had different length, intensity, and source. The first is most likely because of ancient mantle metasomatism, the last is associated with kimberlite activity.

3. The formation of standard kelyphitic rims (Rim1–2) around the peridotitic garnets took place between these stages, before the xenoliths were captured by kimberlite magma. The transformation of Rim1 with the replacement of spinel by magnetite, and silicate minerals by phlogopite (Rim3) was influenced by kimberlite melts.

4. Along with the traditional trends reflecting the change in the composition of spinel from chromite to magnetite (kimberlite and Fe–Ti trends) and from Chromite to Spinel (Cr–Al trend), for mantle xenoliths from kimberlite, the $Al–Fe^{3+}$ trend should be taken into account as inherent in spinel compositions of eclogites, as well as, apparently, playing a key role in the transformation of the rims around the garnet (Rim1 → Rim3).

Conflicts of Interest: The author declares no conflict of interest.

References

1. Irvine, T.N. Chromian Spinel as a Petrogenetic Indicator: Part 1. Theory. *Can. J. Earth Sci.* **1965**, *2*, 648–672. [CrossRef]

2. Irvine, T.N. Chromian Spinel as a Petrogenetic Indicator: Part 2. Petrologic applications. *Can. J. Earth Sci.* **1967**, *4*, 71–103. [CrossRef]

3. Sack, R.O.; Ghiorso, M.S. Chromian Spinels as Petrogenetic Indicators Thermodynamics and Petrological Applications. *Am. Mineral.* **1991**, *76*, 827–847.

4. Arai, S. Chemistry of chromian spinel in volcanic rocks as a potential guide to magma chemistry. *Mineral. Magzine* **1992**, *56*, 173–184. [CrossRef]

5. Power, M.R.; Pirrie, D.; Andersen, J.C.Ø.; Wheeler, P.D. Testing the validity of chrome spinel chemistry as a provenance and petrogenetic indicator. *Geology* **2000**, *28*, 1027–1030. [CrossRef]

6. Barnes, S.J.; Roeder, P.L. The range of spinel compositions in terrestrial mafic and ultramafic rocks. *J. Petrol.* **2001**, *42*, 2279–2302. [CrossRef]

7. Pokhilenko, N.P.; Sobolev, N.V.; Lavrent'ev, Y.G. Xenoliths of diamondiferous ultramafic rocks from Yakutian kimberlites. In Proceedings of the 2nd International Kimberlite Conference, Santa Fe, NM, USA, 3–7 October 1977.

8. Sobolev, N.V.; Pokhilenko, N.P.; Efimova, E.S. Diamond-bearing peridotite xenoliths in kimberlites and the problem of the origin of diamonds. *Geol. Geofiz. (Rus. Geol. Geophys.)* **1984**, *12*, 63–80.

9. Pokhilenko, N.P.; Pearson, D.G.; Boyd, F.R.; Sobolev, N.V. *Megacrystalline Dunites and Peridotites: Hosts for Siberian Diamonds*; Annual Report of Director Geophysical Laboratory; Carnegie Institution: Washington, DC, USA, 1991; pp. 11–18.

10. Pokhilenko, N.P.; Sobolev, N.V. Xenoliths of diamondiferous peridotites from Udachnaya kimberlite pipe, Yakutia. In Proceedings of the of the 4th International Kimberlite Conference, Perth, Australia, 11–15 August 1986; pp. 309–311.

11. Pokhilenko, N.P.; Sobolev, N.V.; Boyd, F.R.; Pearson, D.G.; Shimizu, N. Megacrystalline pyrope peridotites in the lithosphere of the Siberian Platform: Mineralogy, geochemical peculiarities and the problem of their origin. *Russ. Geol. Geophys.* **1993**, *34*, 71–84.

12. Pokhilenko, L.N.; Mal'kovets, V.G.; Kuz'min, D.V.; Pokhilenko, N.P. New Data on the Mineralogy of Megacrystalline Pyrope Peridotite from the Udachnaya Kimberlite Pipe, Siberian Craton, Yakutian Diamondiferous Province. *Dokl. Earth Sci.* **2014**, *454*, 179–184. [CrossRef]

13. McCammon, C.A.; Griffin, W.L.; Shee, S.R.; O'Neill, H.S.C. Oxidation during metasomatism in ultramafic xenoliths from the Wesselton kimberlite. South Africa: Implications for the survival of diamond. *Contrib. Miner. Petrol.* **2001**, *141*, 287–296. [CrossRef]

14. Stachel, T.; Harris, J.W. The origin of cratonic diamonds—Constraints from mineral inclusions. *Ore Geol. Rev.* **2008**, *34*, 5–32. [CrossRef]

15. Kadik, A.A.; Sobolev, N.V.; Zharkova, Y.V.; Pokhilenko, N.P. Redox conditions of formation of diamond-bearing peridotite xenoliths in the Udachnaya kimberlite pipe, Yakutia. *Geochem. Int.* **1990**, *27*, 41–53.

16. Kadik, A.A. Evolution of Earth's redox state during upwelling of carbon-bearing mantle. *Phys. Earth Planet. Inter.* **1997**, *100*, 157–166. [CrossRef]

17. Pokhilenko, L.N. Features of the Fluid Regime of the Lithospheric Mantle of the Siberian Platform (on Xenoliths of Deep Rocks in Kimberlites). Ph.D. Thesis, Institute of the Earth's Crust, SB RAS, Irkutsk, Russia, 3 October 2006. (In Russian)

18. Pokhilenko, L.N.; Pokhilenko, N.P.; Fedorov, I.I.; Tomilenko, A.A.; Usova, L.V.; Fomina, L.N. Fluid regime peculiarities of the lithosphere mantle of the Siberian platform. In Deep-seated Magmatism, Its Sources and Plumes. In Proceedings of the VIII Interntional Conference, Vladivostok, Russia, 2–6 September 2008; Publishing House of the Institute of Geography SB RAS: Irkutsk, Russia, 2008; Volume 1, pp. 122–129. ISBN 978-5-94797-130-9.

19. Pokhilenko, L.N. Particularities of the reaction rims around garnets from the mantle xenoliths of different parageneses (by the example of basic and ultrabasic rocks from Udachnaya kimberlite pipe, Yakutia). In Proceedings of the XXIX International Conference «Ore Potential of Alkaline, Kimberlite and Carbonatite Magmatism» School "Alkaline magmatism of the Earth", Sudak-Moscow, Ukraine-Russia, 14–22 September 2012; pp. 79–82.

20. Pokhilenko, L.N. Mantle metasomatism of megacrystalline peridotites: Chromspinelide and phlogopite from the xenoliths of Udachnaya kimberlite pipe (Yakutia). In Proceedings of the 6th Orogenic Lherzolite Conference, Marrakech, Morocco, 4–15 May 2014.

21. Pokhilenko, L.N. Spinelide from the xenoliths of megacrystalline peridotites of Udachnaya kimberlite pipe (Yakutia). In Proceedings of the XXXIV International Conference "Magmatism of the Earth and related strategic metal deposits", Miass, Russia, 4–9 August 2017; Zaitsev, V.A., Ermolaeva, V.N., Eds.; GEOKHI RAS: Moscow, Russia, 2017; pp. 182–184.

22. Korolyuk, V.N.; Lavrent'ev, Y.G.; Usova, L.V.; Nigmatulina, E.N. JXA-8100 microanalyzer: Accuracy of analysis of rock-forming minerals. *Russ. Geol. Geophys.* **2008**, *49*, 165–168. [CrossRef]

23. Lavrent'ev, Y.G.; Korolyuk, V.N.; Usova, L.V.; Nigmatulina, E.N. Electron probe microanalysis of rock-forming minerals with JXA-8100 electron probe microanalyzer. *Russ. Geol. Geophys.* **2015**, *56*, 1428–1436. [CrossRef]

24. Korolyuk, V.N.; Pokhilenko, L.N. Electron probe determination of trace elements in olivine. *X-Ray Spectrom.* **2014**, *43*, 353–358. [CrossRef]

25. Roeder, P.L. Chromite: From the fiery rain of chondrules to the Kilauea Iki Lava lake. *Can. Mineral.* **1994**, *32*, 729–746.

26. Arai, S. Characterization of spinel peridotites by olivine-spinel compositional relationships: Review and interpretation. *Chem. Geol.* **1994**, *113*, 191–204. [CrossRef]

27. Wood, B.J.; Virgo, D. Upper mantle oxidation state: Ferric iron contents of lherzolite spinels by ^{57}Fe Mössbauer spectroscopy and resultant oxygen fugacities. *Geochim. Cosmochim. Acta* **1989**, *53*, 1277–1291. [CrossRef]

28. Wood, B.J. An experimental test of the spinel peridotite oxygen barometer. *J. Geophys. Res.-Solid Earth* **1990**, *95*, 15845–15851. [CrossRef]

29. Wood, B.J.; Bryndzia, L.T.; Johnson, K.E. Mantle oxidation state and its relationship to tectonic environment and fluid speciation. *Science* **1990**, *248*, 337–345. [CrossRef]

30. Carmichael, I.S. The Redox States of Basic and Silicic Magmas: A Reflection of Their Source Regions? *Contrib. Mineral. Petrol.* **1989**, *106*, 129–141. [CrossRef]

31. O'Neill, H.S.C.; Wood, B.J. An experimental study of Fe-Mg partitioning between garnet and olivine and its calibration as a geothermometer. *Contrib. Mineral. Petrol.* **1979**, *70*, 59–70. [CrossRef]

32. MacGregor, I.D. The system MgO-Al_2O_3-SiO_2: Solubility of Al_2O_3 in enstatite for spinel and garnet peridotite compositions. *Am. Mineral.* **1974**, *59*, 110–119.

33. Finnerty, A.A.; Rigden, S.M. Olivine barometry: Application to pressure estimation for terrestrial and lunar rocks. *Lunar Planet. Sci. Conf.* **1981**, *12*, 279–281.

34. Ryan, C.G.; Griffin, W.L.; Pearson, N.J. Garnet geotherms: Pressure-temperature data from Cr-pyrope garnet xenocrysts in volcanic rocks. *J. Geophys. Res.* **1996**, *101*, 5611–5625. [CrossRef]

35. Canil, D. The Ni-in-garnet geothermometer: Calibration at natural abundances. *Contrib. Mineral. Petrol.* **1999**, *136*, 240–246. [CrossRef]

36. De Hoog, J.C.M.; Gall, L.; Cornell, D.H. Trace-element geochemistry of mantle olivine and application to mantle petrogenesis and geothermobarometry. *Chem. Geol.* **2010**, *270*, 196–215. [CrossRef]

37. Malinovsky, I.Y.; Doroshev, A.M.; Ran, E.N. Stability of chrome-containing garnets of the pyrope-knorringite series. Experimental studies on mineralogy (1974–1975). *Bull. Inst. Geol. Geophys. Novosib. Russ.* **1975**, 110–115.

38. Brey, G.P.; Doroshev, A.M.; Kogarko, L.N. The Join Pyrope-Knorringite: Experimental Constraints for a New Geothermobarometer for Coexisting Garnet and Spinel. *Contrib. Mineral. Petrol.* **1999**, *136*, 240–246.

39. Grütter, H.S.; Latti, D.; Menzies, A. Cr-saturation arrays in concentrate garnet compositions from kimberlite and their use in mantle barometry. *J. Petrol.* **2006**, *47*, 801–820. [CrossRef]

40. Wan, Z.; Coogan, L.A.; Canil, D. Experimental calibration of aluminum partitioning between olivine and spinel as a geothermometer. *Am. Mineral.* **2008**, *93*, 1142–1147. [CrossRef]

41. Kennedy, C.S.; Kennedy, G.C. The Equilibrium Boundary Between Graphite and Diamond. *J. Geophys. Res.* **1976**, *81*, 2467–2470. [CrossRef]

42. Pollack, H.N.; Chapman, D.S. On the regional variation of heat flow, geotherms and lithospheric thickness. *Tectonophysics* **1977**, *38*, 279–296. [CrossRef]

43. Howarth, G.H.; Barry, P.H.; Pernet-Fisher, J.F.; Baziotis, I.P.; Pokhilenko, N.P.; Pokhilenko, L.N.; Bodnar, R.J.; Taylor, L.A.; Agashev, A.M. Superplume metasomatism: Evidence from Siberian mantle xenoliths. *Lithos* **2014**, *184–185*, 209–224. [CrossRef]

44. Pokhilenko, N.P.; Agashev, A.M.; Litasov, K.D.; Pokhilenko, L.N. Carbonatite metasomatism of peridotite lithospheric mantle: Implications for diamond formation and carbonatite-kimberlite magmatism. *Russ. Geol. Geophys.* **2015**, *56*, 280–295. [CrossRef]

45. Pokhilenko, N.P.; Sobolev, N.V.; Kuligin, S.S.; Shimizu, N. Peculiarities of distribution of pyroxenite paragenesis garnets in Yakutian kimberlite and some aspects of the Evolution of the Siberian Craton lithospheric mantle. In Proceedings of the 7th International Kimberlite Conference, Cape Town, South Africa, 11–17 April 1998; Gurney, J.J., et al., Eds.; Red Roof Design: Cape Town, South Africa, 1999; Volume 2, pp. 689–698.

46. Yudin, D.S.; Tomilenko, A.A.; Alifirova, T.A.; Travin, A.V.; Murzintsev, N.G.; Pokhilenko, N.P. Results of 40Ar/39Ar Dating of Phlogopites from Kelyphitic Rims around Garnet Grains (Udachnaya-Vostochnaya Kimberlite Pipe). *Dokl. Earth Sci.* **2016**, *469*, 728–731. [CrossRef]